Atomic Spectroscopy

Article

Iron Isotopic Measurement using Large-Geometry High-Resolution Multi-Collector Inductively Coupled Plasma Mass Spectrometer

Yvtian Lei,[a,b,c] Ming Li,[a,*] Zaicong Wang,[a,b] Yangtao Zhu,[a,b,c] Zhaochu Hu,[a] Yongsheng Liu,[b] and Xinna Chai[b,c]

[a] State Key Laboratory of Geological Processes and Mineral Resources, China University of Geosciences, Wuhan 430074, P. R. China

[b] School of Earth Sciences, China University of Geosciences, Wuhan 430074, P. R. China

[c] Graduate School, China University of Geosciences, Wuhan 430074, P. R. China

Received: *June. 01, 2022;* ***Revised:*** *June. 28, 2022;* ***Accepted:*** *June. 28, 2022;* ***Online:*** *June. 28, 2022;* ***Published:*** *June. 28, 2022.*

DOI: 10.46770/AS.2022. 111

ABSTRACT: High-precision and accurate Fe isotopic analyses are essential for various geological processes. In this study, Fe isotopic measurements were optimized on a large-geometry, high-resolution Nu Plasma 1700 MC-ICP-MS instrument, which can distinguish Ar-related interferences completely as opposed to other general-sized MC-ICP-MS instruments. Under the conditions of high mass resolution, complete separation of Ar-related interference can be achieved. We evaluated the type and intensity of all Ar-related interferences. The effects of the acid molarity, concentration mismatch, residual HCl, and matrix elements were also evaluated. The results demonstrate that the molarity of the acid, residual HCl, and Cr significantly affected the precision of the Fe isotopic measurements. Fe was purified by one-step column anion-exchange separation using the anion resin AG-MP-1M. The long-term external precisions of δ^{56}Fe and δ^{57}Fe were greater than ± 0.03‰ (2SD) and ± 0.06‰ (2SD), respectively. The Fe isotopic compositions of the five geological reference materials measured in this study agreed with previously published data, within uncertainties.

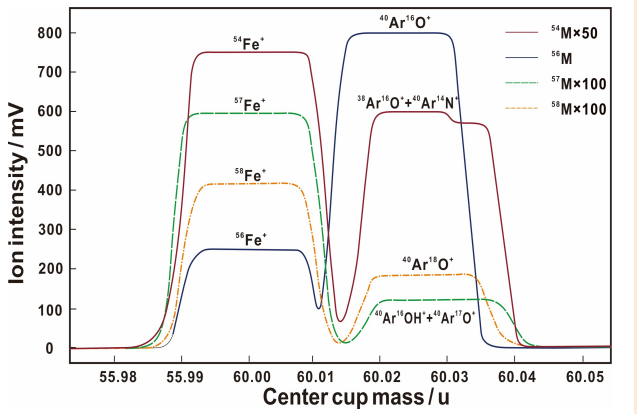

INTRODUCTION

Iron is one of the most abundant elements on Earth and other terrestrial planets, and it is an essential life element for living organisms. Given their importance and recent analytical advances, stable Fe isotopes have received much attention as critical tracers and have been increasingly applied in various scientific disciplines, including astrochemistry,[1-3] geochemistry,[4-6] biology,[7,8] oceanic and environmental science,[9,10] and mineral resources.[11-13] The broad interest in Fe isotopic geochemistry has been mapped out in considerable detail by various special issues and book series, such as the Geochemistry of Non-Traditional Stable Isotopes,[14,15] and Non-Traditional Stable Isotopes.[16]

Iron has four stable isotopes, ^{54}Fe, ^{56}Fe, ^{57}Fe, ^{58}Fe, which represent 5.845, 91.754, 2.1191, and 0.2919 atom% respectively of the total.[17] Mass-dependent isotope variations of Fe in natural samples span a range of ~6‰.[18] Nevertheless, the extent of mass-dependent stable isotope fractionation is a function of both temperature and atomic mass.[19,20] For example, the ranges of Fe isotopic variation in metal/silicate systems (~0.5‰),[21] partial melting (~0.1‰),[22] fractional crystallization (0.1~0.4‰),[16] and melt-peridotite interactions (~1‰)[23] are very narrow. Therefore, the study of Fe isotopes in high-temperature geological processes requires more accurate and precise analytical methods.

Both thermal ionization mass spectrometry (TIMS) and multi-collector inductively coupled plasma mass spectrometry (MC-ICP-MS) can be employed to measure the Fe isotopic composition. Early attainable precisions measured using TIMS have at best been 0.15 ‰/amu.[24] TIMS instruments possess a relatively small bias, but it is highly unstable and cannot be easily corrected.[16] In contrast, MC-ICP-MS instruments are affected by a large instrumental mass bias; however, this bias is more stable than that in TIMS[16] and can be easily corrected by bracketing standards[10,25,26] or by element doping (Cu or Ni).[27-29] Therefore, precisions better than 0.03‰ for δ^{56}Fe could be obtained using MC-ICP-MS.[30] Another advantage of MC-ICP-MS over TIMS, is its high sample throughput, as it is possible to measure up to a few tens of samples per day.[16] MC-ICP-MS has therefore been recognized as the most effective method to determine the Fe isotopic composition.

The mass interference of isobaric polyatomic ions is one of the major disadvantages of MC-ICP-MS. Ar-related interference presents a major challenge to the high-precision measurement of Fe isotopes using MC-ICP-MS. These interferences arise from the Ar gas used to generate the plasma and from N, O, and H present in the atmosphere and solution.[27] Several approaches such as desolvation,[26,31-33] cold plasma,[34] collision cell,[35-37] and high-resolution techniques[28,30,38] have been adopted to address this problem. The consensus is that high mass resolution through optical peak separation is the most robust method to eliminate spectral interferences.[18] At present, only the Nu Plasma series and Neptune series MC-ICP-MS are available, all of which have been successfully used for high-resolution Fe isotopic measurements. Typically, Ar-related interferences and Fe isotopes are sufficiently separated at pseudo medium or high mass resolutions using flat-top peak shoulders (Fig.1).[30,38] The flat top peak shoulder is narrow; therefore, high stability in the magnetic field and the acceleration voltage is essential, both of which are highly sensitive to the temperature of the room.[16] In contrast, Nu Plasma 1700 (Nu Instrument, Wrexham, UK) is a unique, large-geometry high-resolution MC-ICP-MS system that provides ultrahigh mass resolution to allow the complete separation of polyatomic interfering ions.[39,40] Nu Plasma 1700 was tuned to achieve a full baseline separation of the Fe and ArN/O peaks, increasing the accuracy and precision of the results.[28,41]

In this study, based on the ultrahigh mass resolution of Nu Plasma 1700 MC-ICP-MS, the polyatomic interferences of Fe isotopes were measured in detail. The data would be useful for assessing the source of the interference and for searching for mechanisms to eliminate the interference. In addition, we developed an efficient chemical-separation procedure. Fe in the samples was purified through a single ion-exchange column using a strong anionic resin, AG-MP-1M. Only small amounts of acid were required for this process. The effects of the acid molarity, acid residue, concentration mismatch, and matrix elements on the Fe isotopic measurements were carefully evaluated. The Fe isotopic compositions of five well-characterized international reference materials and a pure Fe standard solution were determined. The long-term external precision of δ^{56}Fe (almost three years) was better than ±0.03‰ (two standard deviations, 2SD). The Fe isotope data of all the reference materials measured in this study agree with previous reference values.

Fig. 1 Mass scan performed with Neptune series MC-ICP-MS showing all Fe isotopes and relative polyatomic interferences. The signal of Fe isotopes with interference-free can only be detected on left plateau. The central plateau is composed of Fe isotopes and molecular interferences.[38]

EXPERIMENTAL

Instrument. Fe isotopic measurements were performed using a Nu Plasma 1700 MC-ICP-MS (Nu Instruments, Wrexham, UK) at the State Key Laboratory of Geological Processes and Mineral Resources, China University of Geosciences, Wuhan, China. This instrument is a large-geometry, double-focusing, multi-collector ICP-MS.[39,40] The natural dispersion of the instrument is approximately 1700 mm, which is more than thrice that of other general-sized MC-ICP-MS instruments. The unique design of high dispersion and large geometry allows a high mass resolution of >5000 (10% valley) while maintaining a flat-top peak. The instrument contains 16 Faraday detectors, each of which possesses an independently adjustable slit that can be adjusted with respect to both width and central position, thus allowing different resolutions to be set on individual detectors. These features enable Nu Plasma 1700 to provide a true high mass resolution for fully resolving polyatomic interfering ions.

Fe ions were simultaneously collected using fixed Faraday detectors at *m/z* 54, 56, 57, and 58. Two mechanically adjustable Faraday detectors at *m/z* 52 and 60 were used to monitor the Cr and Ni levels in the samples (Table 1).

The MC-ICP-MS system was run with 1300 W forward RF power using ultrapure Ar (99.999% purity from Air Gas Products) as the plasma and nebulizer gas. A 5 μg g^{-1} Fe solution was introduced into the Ar plasma *via* a Cetac ASX-112FR automatic sampler (CETAC Technologies, Omaha, NE, USA) and a self-aspirating glass expansion micromist nebulizer (Glass Expansion, Pocasset, MA, USA) at an uptake rate of 100 μL min^{-1} producing

Table 1. Instrumental operating conditions for Fe isotopic measurements

Parameters	Values		Parameters	Values		
MC-ICP-MS	Nu Plasma 1700		**Nebulizer**	Glass Expansion, ~ 100 μL min^{-1}		
Cooling Gas	Ar, 13 L min^{-1}		**Cones**	Standard sampling and skimmer cones		
Auxiliary Gas	Ar, 0.95 L min^{-1}		**Mass resolution**	3000 (10% valley)		
Nebulizer Gas	Ar, 30.5 Psi		**Ion transfer rate**	15%		
RF Power	1300 W		**Sensitivity**	^{56}Fe, ~ 5 V ppm^{-1}		
Cup configurations	L6	L4	Ax	H3	H5	H7
m/z	52	54	56	57	58	60
Monitoring	$^{52}Cr^+$	$^{54}Fe^+$ and $^{54}Cr^+$	$^{56}Fe^+$	$^{57}Fe^+$	$^{58}Fe^+$ and $^{58}Ni^+$	$^{60}Ni^+$

a typical signal intensity of ~25 V for ^{56}Fe under the instrumental conditions shown in Table 1.

Mass resolution setting. Nu Plasma 1700 MC-ICP-MS can achieve complete separation of polyatomic interfering ions. Therefore, the mass resolution is defined as the ratio of M/ΔM, where M is the mass measured and ΔM is defined as the peak width at 5% of the peak height. In this case, the two peaks separated by ΔM have a 10% valley between them. The mass resolution given by a 10% valley is approximately equal to the theoretically required resolution to distinguish isotopes from isobaric interferences.[39] The following ions can potentially affect Fe isotopes measured by MC-ICP-MS (Table S1): chromium and nickel; double-charged palladium, cadmium, and tin; polyatomic ions, including argon, oxygen, nitrogen, and hydrogen. The required resolution to separate Fe isotopes from Cr or Ni ions is more than 27000, which cannot be achieved by any contemporary manufactured MC-ICP-MS. The resolutions required to exclude double-charged Pd, Cd, and Sn are in the range 3000–4400. Nu Plasma 1700 can operate at a mass resolution higher than 5000, but in such a case, the ion transmission rate would decrease to less than 10%, thereby affecting the analytical sensitivity. Fortunately, the amounts of these elements in natural samples are very low. Thus, other matrix elements in geological and biological samples can be completely removed following Fe purification. In this study, the instrument was operated at a mass resolution of 3000 (10% valley), while the corresponding ion transmission rate was 15%. In this resolution mode, polyatomic ion interferences such as $^{38}Ar^{16}O^+$, $^{40}Ar^{14}N^+$ on $^{54}Fe^+$, $^{40}Ar^{16}O^+$ on $^{56}Fe^+$, $^{40}Ar^{16}OH^+$, $^{40}Ar^{17}O^+$ on $^{57}Fe^+$, and $^{40}Ar^{18}O^+$ on $^{58}Fe^+$ were fully resolved (Table S1 and Fig. 2a).

Samples and chemical procedure. Five powdered geological reference materials, including three basalts: BHVO-2, BIR-1a and BCR-2; one andesite: AGV-2; and one granodiorite: GSP-2 from the United States Geological Survey (USGS) were analyzed for Fe isotopic compositions. Two Fe reference materials, IRMM-014 and IRMM-524a, were originally provided by the European Institute for Reference Materials and Measurements (IRMM). Stock solutions of IRMM-014 (~ 100 μg g^{-1} Fe) were obtained from Prof. Huang Fang's research group at the University of Science and Technology of China. IRMM-524a (~ 5000 μg g^{-1} Fe in 0.35 mol L^{-1} HNO_3) was prepared by quantitative dissolution of

Fig. 2 Mass scans performed by Nu Plasma 1700 MC-ICP-MS using a mass resolution of 3000 (10% valley) with 50 ng g^{-1} NIST Fe, 1 ng g^{-1} Cr, and 1 ng g^{-1} Ni in 0.35 mol L^{-1} HNO_3 (a); 0.35 mol L^{-1} HNO_3 (b); deionized water (c). Molecular isobaric interferences ($^{38}Ar^{16}O^+$, $^{40}Ar^{14}N^+$, $^{40}Ar^{16}O^+$, $^{40}Ar^{16}OH^+$, $^{40}Ar^{17}O^+$, *etc.*) were completely separated from Fe isotopes.

0.1 mm iron foil using HNO_3. Pure standard solutions, such as NIST Fe (Standard Reference Material 3126a, Lot No. 140812, National Institute of Standards and Technology, Gaithersburg, MD, USA), NIST Cr (Standard Reference Material 3112a, Lot No. 030730), and NIST Ni (Standard Reference Material 3136, Lot No. 120619), were used for condition testing and routine tuning.

All chemical procedures were performed in clean boxes (Class 100) in clean rooms (Class 1000) with HEPA-filtered air at the State Key Laboratory of Geological Processes and Mineral Resources, China University of Geosciences, Wuhan, China. Teflon coated hot plates, Teflon beakers, double distilled hydrochloric, nitric, and hydrofluoric acids, and deionized water (18.2 MΩ cm) were used throughout the experiments to minimize the total procedural blank.

The samples which contained 50-100 μg Fe were weighed into 7 mL Savillex® Teflon vials, to which 1 mL concentrated HNO_3 and 1 mL concentrated HF were added. Following a vibration period of 10 min to avoid caking the powder, the capped vials were placed on a hotplate at 120 °C for 24 h, for sample digestion. The samples were then evaporated to dryness at 120 °C and re-dissolved twice in 1 mL of concentrated HNO_3 to completely remove HF. Subsequently, 0.5 mL of concentrated HNO_3 and 1.5 mL concentrated HCl were added, following which the vials were capped and heated on a hotplate at 120 °C for 12 h. The dissolved samples were evaporated to dryness, re-dissolved in 1 mL concentrated HCl, and heated to dryness. The HCl fluxing procedure was repeated twice to completely convert it into chloride form. Finally, the solutions were dried and then dissolved in 0.5 mL of 8 mol L^{-1} HCl (+0.001% H_2O_2).

The Fe purification was modified according to the method described by Huang *et al*.[42] The 0.8 mL of AG-MP-1M resin was filled into Bio-Rad columns and cleaned by running 2 mL of H_2O, 5 mL of 0.5 mol L^{-1} HNO_3, 2 mL of H_2O, 5 mL of 0.5 mol L^{-1} HCl, and 2 mL of H_2O. Subsequently, 2 mL of 8 mol L^{-1} HCl was added to the column. Then, a 0.5 mL sample solution was loaded onto the resin. Matrix elements such as Ca, Mg, Al, Na, Cr, and Ni were eluted from the column in 5 mL of 8 mol L^{-1} HCl. Fe was then eluted with 4 mL of 0.5 mol L^{-1} HCl and 1 mL of H_2O (Table 2). Following the elution, the Fe solution was dried. It was converted from an HCl to HNO_3 solution by addition and evaporation of 0.5 mL of HNO_3 and 0.5 mL of MQ water, respectively; this sequence was repeated a second time. Finally, the purified samples (Table S2) were preserved in 0.35 mol L^{-1} HNO_3 for isotope analysis. Procedural blank for Fe was less than 20 ng, which was insignificant relative to the amount of Fe put through chemical purification (50-100 μg). This purification is fast and consumes little acid, but it does not separate Cu and Co from Fe. The matrix effects of Cu and Co on Fe isotope analysis need to be discussed later.

Iron isotopic measurement. Iron isotope ratios were measured using the sample-standard bracketing (SSB) method. The dissolved IRMM-014 Fe isotope standard with 5 μg g^{-1} Fe was used as the bracketing standard. Sample solutions (including dissolved IRMM-524a and all test solutions) were typically diluted to 5.00 ± 0.25 μg g^{-1} Fe for analysis. IRMM-524a has the same Fe isotopic composition as IRMM-014.[16,43,44] Given that stocks of IRMM-014 have been exhausted, IRMM-524a has been recommended for normalization in the laboratory; δ-values are expressed relative to IRMM-014.[16]

Table 2. Chromatographic separation procedures of Fe

Steps	Eluent	Volume(mL)
Clean resin	MQ water	2
	0.5 mol L^{-1} HNO_3	5
	MQ water	2
	0.5 mol L^{-1} HCl	5
Condition resin	MQ water	2
	8 mol L^{-1} HCl + 0.001‰ H_2O_2	2
Load sample	8 mol L^{-1} HCl + 0.001‰ H_2O_2	0.5
Remove matrix	8 mol L^{-1} HCl + 0.001‰ H_2O_2	5
Elute Fe	0.5 mol L^{-1} HCl	4
	MQ water	1

Prior to each isotopic analysis, a 60 s on-peak acid blank was measured and subtracted from the analyte signal. Each isotopic analysis included an integration of 25 cycles with 8 s per cycle. During routine measurements, the internal precision was better than 15×10^{-6} (relative standard error) for the $^{56}Fe/^{54}Fe$ ratio.

Fe isotopic compositions were reported using the standard per mil (‰) notation of $\delta^{56}Fe$ for the $^{56}Fe/^{54}Fe$ ratio and $\delta^{57}Fe$ for the $^{57}Fe/^{54}Fe$ ratio, where:

$$\delta^{56}Fe = [(^{56}Fe/^{54}Fe_{sample})/(^{56}Fe/^{54}Fe_{IRMM\text{-}014})\text{-}1] \times 1000$$

$$\delta^{57}Fe = [(^{57}Fe/^{54}Fe_{sample})/(^{57}Fe/^{54}Fe_{IRMM\text{-}014})\text{-}1] \times 1000$$

RESULTS AND DISCUSSION

Ar-related interferences. Ar is necessary to create a radiofrequency (RF) plasma. However, Ar and Ar-related polyatomic isobars have a considerable effect on the generation of high-precision isotopic data pertaining to elements such as potassium,[45] calcium,[39] chromium,[46] iron,[28] and nickel isotopes.[47] Hence, it is necessary to evaluate the type and intensity of all the Ar-related interferences. Benefitting from the high mass resolution, Nu Plasma 1700 could achieve the complete resolution of Ar-related polyatomic ions, providing a convenient research platform to assess the type and intensities of argide interference.[39]

At a mass resolution of 3000 (10% valley), polyatomic ion interferences, such as $^{36}Ar^{16}O^+$ and $^{38}Ar^{14}N^+$ on $^{52}Cr^+$, $^{38}Ar^{16}O^+$, $^{40}Ar^{14}N^+$ and $^{36}Ar^{18}O^+$on $^{54}Fe^+$, $^{40}Ar^{16}O^+$ on $^{56}Fe^+$, $^{40}Ar^{16}OH^+$, $^{40}Ar^{17}O^+$ on $^{57}Fe^+$, and $^{40}Ar^{18}O^+$ on $^{58}Fe^+$ were fully resolved (Fig.

2a). To further evaluate the type and the intensities of Ar-O and Ar-N interferences, three samples, 0.35 mol L^{-1} HNO_3 including 50 ng g^{-1} Fe, 1 ng g^{-1} Cr, and 1 ng g^{-1} Ni (Fig. 2a), pure 0.35 mol L^{-1} HNO_3 (Fig. 2b), and deionized water (Fig. 2c), were mass scanned separately. The intensities of $^{40}Ar^{16}O^+$, $^{40}Ar^{18}O^+$ and the mixed signal intensities of $^{36}Ar^{16}O^+ + {}^{38}Ar^{14}N^+$, $^{38}Ar^{16}O^+ + {}^{40}Ar^{14}N^+ + {}^{36}Ar^{18}O^+$, $^{40}Ar^{14}N^+ + {}^{36}Ar^{18}O^+$, and $^{40}Ar^{16}OH^+ + {}^{40}Ar^{17}O^+$ were obtained directly. The intensities of other polyatomic ions were calculated by assuming that the oxide or hydride yield of each Ar isotope was consistent, while assuming that the mass bias fractionation factors (*f*) during the MC-ICP-MS measurement of Ar and all Ar-related polyatomic isobars were consistent.

The mass bias fractionation factors (*f*) were calculated using the kinetic equilibrium equation:

$$f = ln\left(\frac{(^{40}Ar^{18}O)/(^{40}Ar^{16}O)_{true}}{(^{40}Ar^{18}O)/(^{40}Ar^{16}O)_{meas}}\right)\Big/ln\left(\frac{M(^{40}Ar^{18}O)}{M(^{40}Ar^{16}O)}\right)$$

$$= ln\left(\frac{^{18}O/^{16}O_{true}}{^{18}O/^{16}O_{meas}}\right)\Big/ln\left(\frac{M(^{40}Ar^{18}O)}{M(^{40}Ar^{16}O)}\right)$$

where *true* is the natural abundance ratio, *meas* stands for the measured ratio, and *M* is the mass value (amu).

The intensities of $^{40}Ar^{17}O^+$, $^{36}Ar^{16}O^+$, and $^{36}Ar^{18}O^+$ were calculated using the following equations:

$$\left(\frac{(^{40}Ar^{17}O)}{(^{40}Ar^{16}O)}\right)_{meas}\cdot\left(\frac{M(^{40}Ar^{17}O)}{M(^{40}Ar^{16}O)}\right)^f = \left(\frac{(^{40}Ar^{17}O)}{(^{40}Ar^{16}O)}\right)_{corr} = \left(\frac{^{17}O}{^{16}O}\right)_{ture}$$

$$\left(\frac{(^{36}Ar^{16}O)}{(^{40}Ar^{16}O)}\right)_{meas}\cdot\left(\frac{M(^{36}Ar^{16}O)}{M(^{40}Ar^{16}O)}\right)^f = \left(\frac{(^{36}Ar^{16}O)}{(^{40}Ar^{16}O)}\right)_{corr} = \left(\frac{^{36}Ar}{^{40}Ar}\right)_{ture}$$

$$\left(\frac{(^{36}Ar^{18}O)}{(^{40}Ar^{18}O)}\right)_{meas}\cdot\left(\frac{M(^{36}Ar^{18}O)}{M(^{40}Ar^{18}O)}\right)^f = \left(\frac{(^{36}Ar^{18}O)}{(^{40}Ar^{18}O)}\right)_{corr} = \left(\frac{^{36}Ar}{^{40}Ar}\right)_{ture}$$

where *corr* stands for corrected ratios.

The intensities of $^{38}Ar^{14}N^+$, $^{40}Ar^{14}N^+$, $^{38}Ar^{16}O^+$, and $^{40}Ar^{16}OH^+$ were calculated using the following equations:

$$^{38}Ar^{14}N = \left(^{38}Ar^{14}N + {}^{36}Ar^{16}O\right)_{mix} - {}^{36}Ar^{16}O$$

$$^{40}Ar^{14}N = \left(^{40}Ar^{14}N + {}^{36}Ar^{18}O\right)_{mix} - {}^{36}Ar^{18}O$$

$$^{38}Ar^{16}O = \left(^{38}Ar^{16}O + {}^{40}Ar^{14}N + {}^{36}Ar^{18}O\right)_{mix} - \left(^{40}Ar^{14}N + {}^{36}Ar^{18}O\right)_{mix}$$

$$^{40}Ar^{16}OH = \left(^{40}Ar^{16}OH + {}^{40}Ar^{17}O\right)_{mix} - {}^{40}Ar^{17}O$$

where *mix* stands for mixed signal intensity.

The intensity of $^{40}Ar^{17}OH^+$ was calculated using the following equation:

$$\left(\frac{(^{40}Ar^{17}OH)}{(^{40}Ar^{17}O)}\right)_{meas} = \left(\frac{(^{40}Ar^{16}OH)}{(^{40}Ar^{16}O)}\right)_{meas}$$

Finally, all the intensities of argide interferences that would affect Fe isotopic measurements were clearly identified under the conditions of routine wet plasma mode and 15% ion transmission rate (Table 3). As usual, significant interferences were $^{40}Ar^{16}O^+$ (680~800 mV) on $^{56}Fe^+$, $^{40}Ar^{14}N^+$ (8.9~11.4 mV) on $^{54}Fe^+$, $^{40}Ar^{18}O^+$ (1.5~1.9 mV) on $^{58}Fe^+$, and $^{36}Ar^{16}O^+$ (~2 mV) on $^{52}Cr^+$. Other interferences, such as $^{40}Ar^{16}OH^+$ (~0.9 mV) and $^{40}Ar^{17}O^+$ (~0.3 mV) on $^{57}Fe^+$, $^{38}Ar^{16}O^+$ (~0.65 mV) on $^{54}Fe^+$, and $^{38}Ar^{14}N^+$ (~0.5 mV) on $^{52}Cr^+$ were insignificant. The intensities of the $^{36}Ar^{18}O^+$ (~0.005 mV) and $^{40}Ar^{17}OH^+$ (~0.0004 mV) peaks were negligible.

With the exception of $^{40}Ar^{14}N^+$, the intensities of various Ar-related polyatomic isobars were not significantly different between 0.35 mol L^{-1} HNO_3 and deionized water. The intensity of $^{40}Ar^{14}N^+$ from deionized water was much lower than that from 0.35 mol L^{-1} HNO_3. This trend shows that nitride polyatomic interferences were more significant from HNO_3 than from ambient air.

Effects of acid molarity and concentration mismatch. The molarity of the acid used for Fe isotopic analysis may affect the accuracy of data.[48,49] This potential influence on Fe isotopic analysis was evaluated as follows. A NIST Fe solution was diluted to 5 μg g^{-1} in 0.35 mol L^{-1} HNO_3 to bracket 5 μg g^{-1} NIST Fe solutions diluted by HNO_3 from 0.07 mol L^{-1} to 0.63 mol L^{-1}. Fig. 3a shows an obvious Fe isotopic offset with sample/standard acid molarity ratios ranging from 0.2 to 1.8, indicating that a higher acid molarity would lead to a heavier isotopic composition of Fe.

Table 3. Intensity of molecular isobaric interferences in different matrix

m/z	Molecular ion interferences	50 ng g^{-1} Fe, 1 ng g^{-1} Cr, and 1 ng g^{-1} Ni in 0.35 mol L^{-1} HNO_3	0.35 mol L^{-1} HNO_3	Deionized water
52	$^{36}Ar^{16}O^+$ /mV	2.03	1.99	1.78
	$^{38}Ar^{14}N^+$ /mV	0.47	0.59	0.45
54	$^{38}Ar^{16}O^+$ /mV	0.63	0.68	0.49
	$^{36}Ar^{18}O^+$ /mV	0.0047	0.0047	0.0041
	$^{40}Ar^{14}N^+$ /mV	11.37	8.96	0.72
56	$^{40}Ar^{16}O^+$ /mV	797.9	802.7	688.7
57	$^{40}Ar^{17}O^+$ /mV	0.32	0.32	0.27
	$^{40}Ar^{16}OH^+$ /mV	0.92	0.91	0.65
58	$^{40}Ar^{18}O^+$ /mV	1.83	1.87	1.57
	$^{40}Ar^{17}OH^+$ /mV	0.00037	0.00036	0.00026

μg g^{-1} to 30 μg g^{-1} at certain Fe concentration-based bracketing standards (5 μg g^{-1} NIST Fe). The results demonstrate that Fe isotope analyses appeared only slightly affected when sample/standard concentration ratios were lower than 0.8 or considerably higher than 1.4 (Fig. 3b), while the isotopic offset was still in the precision range. These results are consistent with those of previous studies.[48,49]

Three-isotope plots of acid molarity and concentration mismatch tests are shown in Fig. 3c. These test data did not produce obvious mass-independent fractionation. A few points deviated from the theoretical mass equilibrium (1.475) or kinetic (1.488) fractionation line. This difference might result from the instability of the analytical conditions (acid molarity or concentration).

Therefore, it is crucial to match the acid molarity between the standard and sample. Although the Fe isotopic measurements were observed to be insensitive to concentration, as a good laboratory practice, we adjusted both the sample concentration and acid molarity to be within 5% relative to the standards in routine operation. For each routine analytical sequence, the same batch of 0.35 mol L^{-1} HNO_3 was used to prepare all purified samples and standards. Prior to isotopic measurements, all concentrations of samples and standards were pre-analyzed using a mass spectrometer and diluted to a unified concentration.

Effects of residual hydrochloric acid. A large amount of HCl was used for chromatographic purification of Fe. Therefore, it is crucial to evaluate the effect of residual HCl, which was tested by adding HCl of various molarities to the samples (NIST Fe). We bracketed a series of samples with residual HCl molarity ranging from 0.25 mmol L^{-1} to 50 mmol L^{-1} using the NIST Fe standard at the same concentration (5 μg g^{-1}) and constant acid molarity (adjusting the amount of HNO_3). This result suggests that HCl would lead to a heavier isotopic composition of Fe when the HCl concentration was greater than 10 mmol L^{-1} (Fig. 4). The 50 mmol L^{-1} residual HCl in the samples resulted in a shift of more than 0.2‰ in $\delta^{56}Fe$. Consequently, the conversion of HCl to HNO_3 is essential for accurate Fe isotopic determination.

Effect of elemental matrix. The matrix elements present in sample solutions can affect Fe isotopic determinations. In this study, several major and trace matrix elements were assessed for their potential impact on Fe isotopic measurements. The samples (NIST Fe; 5 μg g^{-1}) were mixed with various quantities of matrix elements; these solutions were measured against a 5 μg g^{-1} pure NIST Fe solution. The resulting $\delta^{56}Fe$ data are presented in Fig. S1 against the concentration ratios of matrix elements to Fe (C_{matrix}/C_{Fe}). The effect of the matrix elements on Fe isotopes was negligible when $C_{(V, Ti)}/C_{Fe} < 0.001$, $C_{(K, Ca, Ni, Mn)}/C_{Fe} < 0.01$, $C_{Al}/C_{Fe} < 0.02$, and $C_{(Zn, Mg)}/C_{Fe} < 0.1$. No obvious deviation in $\delta^{56}Fe$ was observed when C_{Na}/C_{Fe} was less than 0.2. It was crucial to test the specific impact of Cu and Co given that they are not

Fig. 3 Effects of mismatch of acid molarity (a) and Fe concentration (b) on Fe isotopic analyses. And plot of $\delta^{56}Fe$ vs $\delta^{57}Fe$ of acid molarity and concentration mismatch test (c). The gray area represents the long-term external uncertainty of ± 0.03‰ (2SD) for $\delta^{56}Fe$.

Fig. 4 Effects of residual HCl on Fe isotopic analyses. The gray area represents the long-term external uncertainty of ± 0.03‰ (2SD) for $\delta^{56}Fe$.

The effect of the Fe concentration mismatch between standards and samples on Fe isotopic measurements was also evaluated. We tested this by varying the Fe concentration of the samples from 2

Fig. 5 Effects of Cr on Fe isotopic analyses. There is a good agreement between the actual test values (blue spot) and the simulated values (gray dotted line). The simulated values were based on the natural abundances of Cr and Fe modeling. The gray area represents the long-term external uncertainty of ± 0.03‰ (2SD) for δ^{56}Fe.

separated from Fe in the chromatographic procedure. The results demonstrate that there is no significant offset when $C_{Cu}/C_{Fe} < 0.02$ or $C_{Co}/C_{Fe} < 0.02$ (Fig. S1). Notably, this Fe purification is not suitable for copper-rich or cobalt-rich samples such as copper ore and cobalt nodules.

Although Cr was eluted completely during the Fe purification process (Table S2), the influence of Cr was also evaluated. Different amounts of Cr were added to 5 μg g^{-1} NIST Fe solution. The results demonstrated that if C_{Cr}/C_{Fe} was less than 0.0001, a detectable bias could not be produced in the Fe isotopic analyses (Fig. 5). In addition, we simulated the effect of Cr on Fe, which is indicated by the gray dotted line in Fig. 5. The line was based on the natural abundances of Cr and Fe modeling. It was in good agreement with the test value, and all of them suggested that a higher Cr/Fe ratio (> 0.0001) can yield a significantly lighter Fe isotope composition. The accuracy of the Fe isotopic analysis requires Cr interference monitoring through the detection of ^{52}Cr during testing.

Iron isotopic compositions of geological standards. Five igneous rock reference standards, including three basalts (BHVO-2, BIR-1a, and BCR-2), one andesite (AGV-2), and one granodiorite (GSP-2), were analyzed in this study. The long-term reproducibility of the Fe isotopic analysis was evaluated by replicating measurements of these geological reference materials, bracketed with standard IRMM-014 over a period of more than three years. The external precision of the measurements was better than ± 0.03‰ (2SD) and ± 0.06‰ (2SD) for δ^{56}Fe and δ^{57}Fe, respectively (Fig. 6).

The Fe isotopic compositions of these reference materials were consistent with previously recommended values published in other studies, within statistical uncertainties (Fig. 6).[43,48,49] Overall, the results of these tests confirm the accuracy and precision of Fe isotopic analyses using the chemical purification and instrumental measurement methods proposed in this study.

Fig. 6 Long-term analyses of IRMM-524a and USGS geological reference materials (BIR-1a, BCR-2, BHVO-2, AGV-2, GSP-2) relative to IRMM-014. The long-term external precisions were better than ± 0.03 ‰ (2SD) and ± 0.06 ‰ (2SD) for δ^{56}Fe and δ^{57}Fe respectively.

Fig. 7 Plot of $\delta^{56}Fe$ vs $\delta^{57}Fe$ of measured geological reference materials. The results define a linear trend with a slope of 1.497 ± 0.019, which is similar to both theoretically equilibrium fractionation value ($(1/m^{57}Fe\text{-}1/m^{54}Fe)/(1/m^{56}Fe\text{-}1/m^{54}Fe)$, 1.475) and kinetic fractionation value ($\ln(m^{57}Fe/m^{54}Fe)/\ln(m^{56}Fe/m^{54}Fe)$, 1.488), m is the relative atomic weight of Fe isotopes.

Three-isotope plots of the five USGS geological standards are shown in Fig. 7. The data obtained for these reference materials yielded a $\delta^{57}Fe$ versus $\delta^{56}Fe$ fractionation line, with a slope of 1.497 ± 0.019. This slope value was indistinguishable from the equilibrium (1.475) or kinetic (1.488) fractionation law within statistical error. This indicates that there are no obvious contributions of unresolved isobaric interferences to Fe isotopic analyses.

CONCLUSIONS

A high-precision Fe isotopic analysis method using sample-standard bracketing was presented using a Nu 1700 MC-ICP-MS. The high mass resolution (3000; 10% valley) of this instrument for Fe isotopic measurements achieved complete resolution and elimination of Ar-related interferences. This allowed us to evaluate the type and intensity of all the Ar-related interferences.

Fe was purified from the samples using the anion resin AG-MP-1M in a single column. Most matrix elements (Cu, Zn, Co, K, Ca, Mg, Al, Na, Mn, and Ti) had no significant effect on Fe isotopic analyses. Although Cr can substantially affect the ^{54}Fe measurement, it was removed efficiently through chromatographic separation in this study. Because of the obvious influence of acid mismatch, the acid molarity of both the samples and standards was kept consistent with one another, while it was ensured that no residual HCl remained in the solutions. Although Fe isotopic analyses are not sensitive to concentration matching, a difference within 5% was maintained relative to the applicable standards.

Based on repeated analyses of the geological reference materials, the long-term external precisions of $\delta^{56}Fe$ and $\delta^{57}Fe$ were better than ± 0.03‰ and ± 0.06‰ (2SD), respectively. All Fe isotopic data obtained in this study were consistent with previously published values, within statistical uncertainty.

ASSOCIATED CONTENT

The supporting information (Fig. S1, Table S1 and S2) is available at www.atspectrosc.com/as/home

AUTHOR INFORMATION

Ming Li is a senior engineer at the State Key Laboratory of Geological Processes and Mineral Resources, China University of Geosciences (Wuhan), China. He received his Ph.D. in geochemistry from the China University of Geosciences (Wuhan) in 2010. His major research interests are analytical geochemistry, geochemical microanalysis, and metal stable isotope analysis. He is the lab manager of the Nu Plasma 1700 MC-ICP-MS lab. He is responsible for the operation and management of Nu Plasma 1700 and analytical method development of the metal stable isotope analysis.

Corresponding Author

*M. Li

Email address: liming19820426@163.com

Notes

The authors declare no competing financial interest.

ACKNOWLEDGMENTS

The authors thank Prof. Huang Fang's research group for providing IRMM-014 standard solutions. This research was co-supported by the National Key R&D Programs of China (2019YFA0708401), the Natural Science Foundation of Hubei Province (2020CFA045), and the most special fund from the State Key Laboratory of Geological Processes and Mineral Resources, China University of Geosciences.

REFERENCES

1. J. A. Barrat, O. Rouxel, K. Wang, F. Moynier, A. Yamaguchi, A. Bischoff, and J. Langlade, *Earth Planet. Sci. Lett.*, 2015, **419**, 93–100. https://doi.org/10.1016/j.epsl.2015.03.026
2. D. C. Hezel, J. S. Wilden, D. Becker, S. Steinbach, F. Wombacher, and M. Harak, *Earth Planet. Sci. Lett.*, 2018, **490**, 31–39. https://doi.org/10.1016/j.epsl.2018.03.013

3. S. Weyer, A. D. Anbar, G. P. Brey, C. Münker, K. Mezger, and A. B. Woodland, *Earth Planet. Sci. Lett.*, 2005, **240**, 251–264. https://doi.org/10.1016/j.epsl.2005.09.023
4. F. Z. Teng, N. Dauphas, S. C. Huang, and B. Marty, *Geochim. Cosmochim. Ac.*, 2013, **107**, 12–26. https://doi.org/10.1016/j.gca.2012.12.027
5. S. Weyer and D. A. Ionov, *Earth Planet. Sci. Lett.*, 2007, **259**, 119–133. https://doi.org/10.1016/j.epsl.2007.04.033
6. M. L. M. Gleeson, S. A. Gibson, and H. M. Williams, *Earth Planet. Sci. Lett.*, 2020, **535**, 116114. https://doi.org/10.1016/j.epsl.2020.116114
7. B. L. Beard, C. M. Johnson, L. Cox, H. Sun, K. H. Nealson, and C. Aguilar, *Science*, 1999, **285**, 1889–1892. https://doi.org/10.1126/science.285.5435.1889
8. M. Guelke-Stelling and F. von Blanckenburg, *Plant Soil*, 2012, **352**, 217–231. https://doi.org/10.1007/s11104-011-0990-9
9. S. Levasseur, M. Frank, J. R. Hein, and A. N. Halliday, *Earth Planet. Sci. Lett.*, 2004, **224**, 91–105. https://doi.org/10.1016/j.epsl.2004.05.010
10. B. L. Beard, C. M. Johnson, K. L. Von Damm, and R. L. Poulson, *Geology*, 2003, **31**, 629–632. https://doi.org/10.1130/0091-7613(2003)031<0629:IICOFC>2.0.CO;2
11. Z.-W. He, X.-C. Zhang, X.-D. Deng, H. Hu, Y. Li, H. Yu, C. Archer, J. Li, and F. Huang, *Geochim. Cosmochim. Ac.*, 2020, **270**, 61–83. https://doi.org/10.1016/j.gca.2019.10.039
12. L. D. Bilenker, A. C. Simon, M. Reich, C. C. Lundstrom, N. Gajos, I. Bindeman, F. Barra, and R. Munizaga, *Geochim. Cosmochim. Ac.*, 2016, **177**, 94–104.
13. J.-X. Li, K.-Z. Qin, G.-M. Li, N. J. Evans, F. Huang, and J.-X. Zhao, *Geochim. Cosmochim. Ac.*, 2018, **238**, 1–15. https://doi.org/10.1016/j.gca.2018.07.008
14. B. L. Beard and C. M. Johnson, *Rev. Mineral. Geochem.*, 2004, **55**, 319–357. https://doi.org/10.2138/gsrmg.55.1.319
15. C. M. Johnson, B. L. Beard, E. E. Roden, D. K. Newman, and K. H. Nealson, *Rev. Mineral. Geochem.*, 2004, **55**, 359–408. https://doi.org/10.2138/gsrmg.55.1.359
16. N. Dauphas, S. G. John, and O. Rouxel, *Rev. Mineral. Geochem.*, 2017, **82**, 415–510. http://doi.org/10.2138/rmg.2017.82.11
17. M. Berglund and M. E. Wieser, *Pure Appl. Chem.*, 2011, **83**, 397–410. https://doi.org/10.1351/PAC-REP-10-06-02
18. N. Dauphas and O. Rouxel, *Mass Spectrom. Rev.*, 2006, **25**, 515–550. https://doi.org/10.1002/mas.20078
19. J. Bigeleisen and M. G. Mayer, *J. Chem. Phys.*, 1947, **15**, 261–267. https://doi.org/10.1063/1.1746492
20. H. C. Urey, *J. Chem. Soc. (Resumed)*, 1947, 562–581. https://doi.org/10.1039/JR9470000562
21. A. Shahar and E. D. Young, *Chem. Geol.*, 2020, **554**, 119800. https://doi.org/10.1016/j.chemgeo.2020.119800
22. S. Weyer and D. A. Ionov, *Earth Planet. Sci. Lett.*, 2007, **259**, 119–133. https://doi.org/10.1016/j.epsl.2007.04.033
23. X. M. Zhao, H. F. Zhang, X. K. Zhu, S. H. Tang, and B. Yan, *Chem. Geol.*, 2012, **292**, 127–139. https://doi.org/10.1016/j.chemgeo.2011.11.016
24. C. M. Johnson and B. L. Beard, *Int. J. Mass Spectrom.*, 1999, **19**, 87–99. https://doi.org/10.1016/S1387-3806(99)00158-X
25. F. Albarede and B. Beard, *Rev. Mineral. Geochem.*, 2004, **55**, 113–152. https://doi.org/10.2138/gsrmg.55.1.113
26. N. S. Belshaw, X. K. Zhu, Y. Guo, and R. K. O'Nions, *Int. J. Mass Spectrom.*, 2000, **197**, 191–195. https://doi.org/10.1016/S1387-3806(99)00245-6
27. G. L. Arnold, S. Weyer, and A. D. Anbar, *Anal. Chem.*, 2004, **76**, 322–327. https://doi.org/10.1021/ac034601v
28. K. Y. Chen, H. L. Yuan, P. Liang, Z. A. Bao, and L. Chen, *Int. J. Mass Spectrom.*, 2017, **421**, 196–203. https://doi.org/10.1016/j.ijms.2017.07.002
29. F. Poitrasson and R. Freydier, *Chem. Geol.*, 2005, **222**, 132–147. https://doi.org/10.1016/j.chemgeo.2005.07.005
30. N. Dauphas, A. Pourmand, and F. Z. Teng, *Chem. Geol.*, 2009, **267**, 175–184. https://doi.org/10.1016/j.chemgeo.2008.12.011
31. A. D. Anbar, J. E. Roe, J. Barling, and K. H. Nealson, *Science*, 2000, **288**, 126–128. https://doi.org/10.1126/science.288.5463.126
32. X. K. Zhu, Y. Guo, R. J. P. Williams, R. K. O'Nions, A. Matthews, N. S. Belshaw, G. W. Canters, E. C. D. Waal, U. Weser, B. K. Burgess, and B. Salvato, *Earth Planet. Sci. Lett.*, 2002, **200**, 47–62. https://doi.org/10.1016/S0012-821X(02)00615-5
33. J. de Jong, V. Schoemann, J. L. Tison, S. Becquevort, F. Masson, D. Lannuzel, J. Petit, L. Chou, D. Weis, and N. Mattielli, *Anal. Chim. Acta*, 2007, **589**, 105–119. https://doi.org/10.1016/j.aca.2007.02.055
34. K. Kehm, E. H. Hauri, C. M. O'D. Alexander, and R. W. Carlson, *Geochim. Cosmochim. Ac.*, 2003, **67**, 2879–2891. https://doi.org/10.1016/S0016-7037(03)00080-2
35. B. L. Beard, C. M. Johnson, J. L. Skulan, K. H. Nealson, L. Cox, and H. Sun, *Chem. Geol.*, 2003, **195**, 87–117. https://doi.org/10.1016/S0009-2541(02)00390-X
36. O. Rouxel, N. Dobbek, J. Ludden, and Y. Fouquet, *Chem. Geol.*, 2003, **202**, 155-182. https://doi.org/10.1016/j.chemgeo.2003.08.011
37. N. Dauphas, P. E. Janney, R. A. Mendybaev, M. Wadhwa, F. M. Richter, A. M. Davis, M. van Zuilen, R. Hines, and N. Foley, *Anal. Chem.*, 2004, **76**, 5855–5863. https://doi.org/10.1021/ac0497095
38. S. Weyer and J. B. Schwieters, *Int. J. Mass Spectrom.*, 2003, **226**, 355–368. https://doi.org/10.1016/S1387-3806(03)00078-2
39. M. Li, Y. Lei, L. P. Feng, Z. C. Wang, N. S. Belshaw, Z. C. Hu, Y. S. Liu, L. Zhou, H. H. Chen, and X. N. Chai, *J. Anal. At. Spectrom.*, 2018, **33**, 1707–1719. https://doi.org/10.1039/c8ja00234g
40. Y. T. Zhu, M. Li, Z. C. Wang, Z. Q. Zou, Z. C. Hu, Y. S. Liu, L. Zhou, and X. N. Chai, *At. Spectrosc.*, 2019, **40**, 206–214. https://doi.org/10.46770/as.2019.06.002
41. H. M. Williams, A. H. Peslier, C. Mccammon, A. N. Halliday, S. Levasseur, N. Teutsch, and J. P. Burg, *Earth Planet. Sci. Lett.*, 2005, **235**, 435–452. https://doi.org/10.1016/j.epsl.2005.04.020
42. F. Huang, Z. F. Zhang, C. C. Lundstrom, and X. C Zhi, *Geochim. Cosmochim. Ac.*, 2011, **75**, 3318–3334. https://doi.org/10.1016/j.gca.2011.03.036
43. P. R. Craddock and N. Dauphas, *Geostand. Geoanal. Res.*, 2011, **35**, 101–123. https://doi.org/10.1111/j.1751-908X.2010.00085.x
44. C. G. de Vega, S. M. Chernonozhkin, R. Grigoryan, M. Costas-Rodríguez, and F. Vanhaecke, *J. Anal. At. Spectrom.*, 2020, **35**, 2517–2529. https://doi.org/10.1039/D0JA00225A
45. X. Q. Li, G. L. Han, Q. Zhang, and Z. Miao, *J. Anal. At. Spectrom.*, 2020, **35**, 1330–1339. https://doi.org/10.1039/D0JA00127A
46. J. M. Zhu, G. L. Wu, X. L. Wang, G. L. Han, and L. X. Zhang, *J. Anal. At. Spectrom.*, 2018, **33**, 809–821. https://doi.org/10.1039/C8JA00033F
47. G. L. Wu, J. M. Zhu, X. L. Wang, G. L. Han, D. C. Tan, and S. J. Wang, *J. Anal. At. Spectrom.*, 2019, **34**, 1639–1651. https://doi.org/10.1039/C9JA00077A
48. Y. S. He, S. Ke, F. Z. Teng, T. T. Wang, H. J. Wu, Y. H. Lu, and S. G Li, *Geostand. Geoanal. Res.*, 2015, **39**, 341–356. https://doi.org/10.1111/j.1751-908X.2014.00304.x
49. S. A. Liu, D. D. Li, S. G. Li, F. Z. Teng, K. Shan, Y. S. He, and Y. H. Lu, *J. Anal. At. Spectrom.*, 2013, **29**, 122–133. https://doi.org/10.1039/c3ja50232e